Inorganic Chemistry

ARTICLE

pubs.acs.org/IC

Synthesis, Structure, Chemical Stability, and Electrical Properties of Nb-, Zr-, and Nb-Codoped $BaCeO_3$ Perovskites

Surinderjit Singh Bhella,[†] Tobias Fürstenhaupt,[‡] Reginald Paul,*[,†] and Venkataraman Thangadurai*[,†]

[†]Department of Chemistry, University of Calgary, 2500 University Drive Northest, Calgary, Alberta, Canada T2N 1N4

[‡]Microscopy and Imaging Facility, University of Calgary, 3330 Hospital Drive Northwest, Calgary, Alberta, T2N 4N1 Canada

Supporting Information

ABSTRACT: We report the effect of donor-doped perovskite-type $BaCeO_3$ on the chemical stability in CO_2 and boiling H_2O and electrical transport properties in various gas atmospheres that include ambient air, N_2, H_2, and wet and dry H_2. Formation of perovskite-like $BaCe_{1-x}Nb_xO_{3\pm\delta}$ and $BaCe_{0.9-x}Zr_xNb_{0.1}O_{3\pm\delta}$ (x = 0.1; 0.2) was confirmed using powder X-ray diffraction (XRD) and electron diffraction (ED). The lattice constant was found to decrease with increasing Nb in $BaCe_{1-x}Nb_xO_{3\pm\delta}$, which is consistent with Shannon's ionic radius trend. Like $BaCeO_3$, $BaCe_{1-x}Nb_xO_{3\pm\delta}$ was found to be chemically unstable in 50% CO_2 at 700 °C, while Zr doping for Ce improves the structural stability of $BaCe_{1-x}Nb_xO_{3\pm\delta}$. AC impedance spectroscopy was used to estimate electrical conductivity, and it was found to vary with the atmospheric conditions and showed mixed ionic and electronic conduction in H_2-containing atmosphere. Arrhenius-like behavior was observed for $BaCe_{0.9-x}Zr_xNb_{0.1}O_{3\pm\delta}$ at 400−700 °C, while Zr-free $BaCe_{1-x}Nb_xO_{3\pm\delta}$ exhibits non-Arrhenius behavior at the same temperature range. Among the perovskite-type oxides investigated in the present work, $BaCe_{0.8}Zr_{0.1}Nb_{0.1}O_{3\pm\delta}$ showed the highest bulk electrical conductivity of 1.3×10^{-3} S cm^{-1} in wet H_2 at 500 °C, which is comparable to CO_2 and H_2O unstable high-temperature Y-doped $BaCeO_3$ proton conductors.

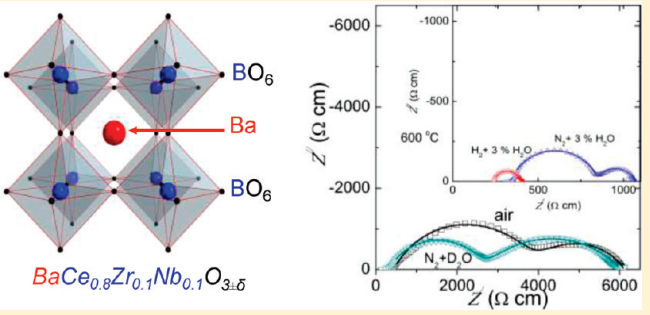

INTRODUCTION

A large number of perovskite and related structure metal oxides have been investigated as potential solid-state proton conductors (SSPCs)[1−7] to replace organic polymer Nafion in conventional proton exchange membrane fuel cells (PEMFCs). Nafion conducts protons under fully hydrated conditions, and the sulfonated framework assists the transport of protons.[8] SSPCs exhibit several advantages over polymer Nafion, including high proton conductivity under low humidity and chemical stability at high temperatures, thus allowing substitution of expensive Pt electrocatalysts with cheap metal oxides. Well-known Y-doped $BaCe_{1-x}Y_xO_{3-\delta}$ (BCY) and B-site nonstoichiometric double-perovskite-type $Ba_3Ca_{1+x}Nb_{2-x}O_{9-\delta}$ (BCN) exhibit proton conductivity at elevated temperatures in H_2O-containing atmospheres.[9−21] The chemical doping mechanism in these oxides could be expressed using Kroger−Vink notations as

$$Y_2O_{3(s)} \rightarrow 2Y'_{Ce(s)} + V^{\bullet\bullet}_{O(s)} + 3O^{X}_{O(s)} \quad (1)$$

$$2CaO_{(s)} \rightarrow 2Ca'''_{Nb(s)} + 3V^{\bullet\bullet}_{O(s)} + 2O^{x}_{O(s)} \quad (2)$$

where $Y'_{Ce(s)}$, $Ca'''_{Nb(s)}$, and $O^{x}_{O(s)}$ represent the Y atom at the Ce site, Ca atom at the Nb site, and oxygen atom at the regular oxygen site, respectively. Generally, oxide-ion vacancy ($V^{\bullet\bullet}_{O}$) is responsible for the oxide-ion conduction at high temperatures, but under H_2O environment, these oxygen vacancies help in the hydration of the structure,[5,6] which leads to the formation of mobile hydroxyl protons ($OH^{\bullet}_{o}$), i.e., $H_2O_{(g)} + V^{\bullet\bullet}_{O(s)} + O^{x}_{o(s)} \rightarrow 2OH^{\bullet}_{o(s)}$.

Our recent[22] chemical stability tests of $BaCe_{1-x}In_xO_{3-\delta}$ (x = 0.1, 0.2), $BaCe_{0.8}Gd_{0.15}Pr_{0.05}O_{3-\delta}$, $BaCe_{0.85}Sm_{0.15}O_{3-\delta}$, and $BaCe_{0.85}Eu_{0.15}O_{3-\delta}$ under CO_2 and H_2O showed the same reaction products, $BaCO_3$ and $Ba(OH)_2$, respectively. Attempts have been made to improve the chemical stability of BCY perovskites using Zr substitution for Ce, but the proton conductivity decreases with increasing Zr content in BCY.[23,24] Accordingly, there is a need for the development of new proton conductors with improved stability and proton conductivity for application in fuel cells. In the present work, we investigate the changes in the electrical conductivity as a consequence of doping pentavalent Nb^{5+} for Ce^{4+} in $BaCeO_3$. To the best of our knowledge, the nominal composition of $BaCe_{0.5}Nb_{0.5}O_3$ has been synthesized previously to determine its dielectric properties.[25]

Received: December 14, 2010
Published: June 21, 2011

EXPERIMENTAL SECTION

Synthesis and Structure of Nb, Nb+Zr-Codoped $BaCeO_3$. The perovskite oxides with nominal chemical formulas of $BaCe_{1-x}Nb_xO_{3\pm\delta}$ and $BaCe_{0.9-x}Zr_xNb_{0.1}O_{3\pm\delta}$ (x = 0.1, 0.2) were prepared by solid-state (ceramic) reactions using appropriate amounts of high-purity $Ba(NO_3)_2$ (99+%, Alfa Aesar), CeO_2 (99%, Fisher Scientific), Nb_2O_5 (99.5%, Alfa Aesar), and ZrO_2 (99.85%, Alfa Aesar) in air. These powders were mixed using a ball mill (Pulverisette, Fritsch, Germany) for 6 h at 200 rpm using zirconia balls and 2-propanol with an intermediate change in rotation direction every hour to ensure proper mixing. The powders were then dried and sintered in air at 900 °C for 12 h in a clean alumina crucible. The resulting mixture was ball milled again for about 6 h and then pressed into pellets (~1 cm diameter, ~2 cm thick) using isostatic pressure. The pressed pellets were sintered at 1500 °C for 24 h in air. The pellets were then ground into a powder for X-ray characterization (PXRD) using a Bruker D8 powder X-ray diffractometer (Cu Kα, 40 kV; 40 mA) at room temperature with a 2θ step scan width of 0.02 and a counting time of 6 s. The lattice constant was determined from the PXRD data by the least-squares refinement method. Chemical stability was determined on the powdered samples in N_2 + CO_2 (50:50) environment at 700 °C for 20 h and in boiling H_2O for 24 h. The resultant products were examined by PXRD and FTIR (NEXUS 470 FT-IR Spectrometer). For FTIR measurements, the KBr powder was kept continuously at about 100 °C in a vacuum oven. Electron paramagnetic resonance (EPR) spectra were recorded at 1300−3600 G and 108 K with a Bruker EMX10/12 instrument equipped with a variable-temperature accessory and gaussmeter.

TEM and Electron Diffraction Studies. The transmission electron microscopy (TEM) coupled with electron diffraction (ED) was done on a FEI Tecnai F20 FEG-TEM (FEI, Eindhoven, The Netherlands) equipped with a Gatan Imaging Filter and a Gatan 860 GIF 2001 CCD of 1024 × 1024 resolution for the as-prepared $BaCe_{1-x}Nb_xO_{3\pm\delta}$ and $BaCe_{0.9-x}Zr_xNb_{0.1}O_{3\pm\delta}$. Standard TEM was done at magnifications between 8000 and 67 000, and HRTEM was performed between 940 000 and 1 350 000. The ED was taken at a camera length of 400 mm, and directly after taking each individual diffraction pattern of the sample, it was exchanged by a reference sample of amorphous Au without changing any settings on the microscope. The diffraction rings of this amorphous gold were used to confirm a proper calibration in diffraction mode of the equipment.

AC Impedance Characterization. Electrical conductivity measurements using porous Pt electrodes were performed in air, wet N_2, wet H_2, and D_2O-saturated N_2. Pt paste (Heraeus Inc., LP A88-11S, Germany) was applied using a paintbrush to both sides of the sintered pellets and cured at 900 °C for 1 h in air to remove the organic binders. Pt wires were attached to the surface of the pellet using a spring-loaded contact, which served as a current collector. The cell was heated to the desired temperature in the range of 300−700 °C using a Barnstead tubular furnace (model 21100) and held at a constant temperature prior to each measurement for a minimum of 2 h and a maximum of 48 h. AC impedance spectroscopy (Solartron Electrochemical Impedance Spectroscopy; SI1260, 100 mV; 0.01−1 MHz) was used to determine the conductivity. A two-probe electrochemical cell was employed for electrical characterization. The conductivity of each sample was measured by subsequent heating and cooling cycles. Desired pH_2O was obtained by keeping the water at a selected temperature (24, 60, and 80 °C) and using N_2 as a carrier gas.

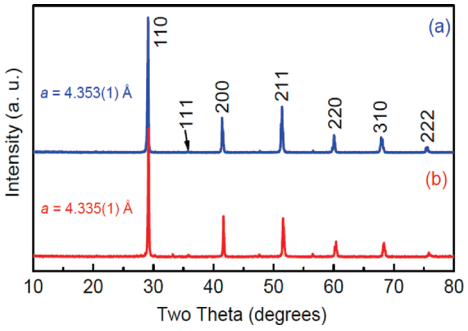

Figure 1. PXRD of (a) $BaCe_{0.9}Nb_{0.1}O_{3\pm\delta}$ and (b) $BaCe_{0.8}Nb_{0.2}O_{3\pm\delta}$ prepared at 1500 °C in air.

RESULTS AND DISCUSSION

Phase Formation and Chemical Stability. PXRD and ED of $BaCe_{1-x}Nb_xO_{3\pm\delta}$ and $BaCe_{0.9-x}Zr_xNb_{0.1}O_{3\pm\delta}$ (Figures 1−4) confirmed the formation of single-phase perovskite-type structure. We could index all of the major diffraction lines based on a simple cubic perovskite (ABO_3) cell ($BaCe_{1-x}Nb_xO_{3\pm\delta}$ a = 4.353(1) Å

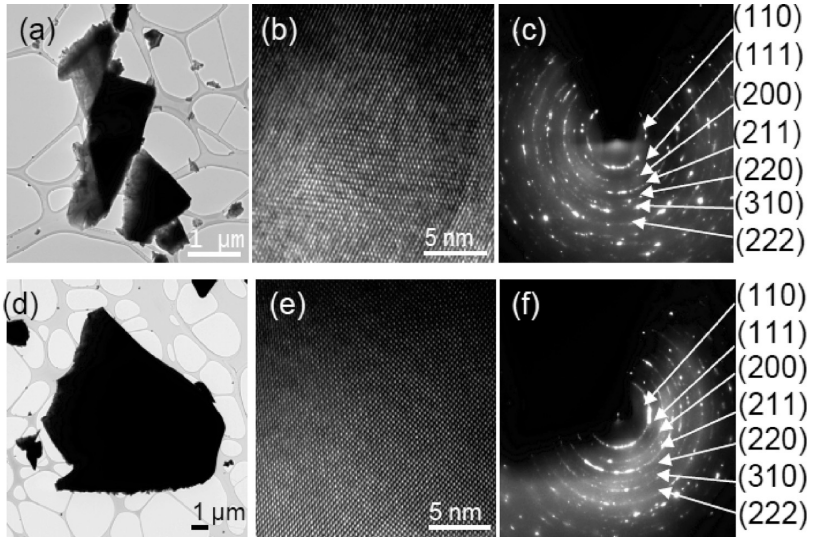

Figure 2. $BaCe_{0.9}Nb_{0.1}O_{3\pm\delta}$ (a−c) and $BaCe_{0.8}Nb_{0.2}O_{3\pm\delta}$ (d−f) show the corresponding TEM and HRTEM images and selected area ED of the sample prepared at 1500 °C in air.

dx.doi.org/10.1021/ic201008v |Inorg. Chem. 2011, 50, 6493–6499

for $x = 0.1$; $a = 4.335(1)$ Å for $x = 0.2$; $BaCe_{0.9-x}Zr_xNb_{0.1}O_{3\pm\delta}$ $a = 4.338(1)$ Å for $x = 0.1$; $a = 4.321(1)$ Å for $x = 0.2$). The measured lattice parameter was found to be comparable to those of the previously reported perovskite-like structure $BaCe_{0.5}Nb_{0.5}O_3$ ($a = 4.293$ Å).[25] Figures 5 and S1 (see Supporting Information) show the chemical stability in $N_2 + CO_2$ (50:50) and in boiling H_2O of $BaCe_{0.9-x}Zr_xNb_{0.1}O_{3\pm\delta}$ and $BaCe_{1-x}Nb_xO_{3\pm\delta}$, respectively. We clearly observed that the $BaCe_{1-x}Nb_xO_{3\pm\delta}$ composition was unstable in CO_2 (Figure S1), while $BaCe_{0.9-x}Zr_xNb_{0.1}O_{3\pm\delta}$ compounds (Figure 5) were found to be robust against chemical reaction with CO_2 at elevated temperatures. Figures 6 and S2 (see Supporting Information) show the FTIR spectra of as-prepared and CO_2- and H_2O-treated $BaCe_{0.8}Zr_{0.1}Nb_{0.1}O_{3\pm\delta}$ and $BaCe_{0.7}Zr_{0.2}Nb_{0.1}O_{3\pm\delta}$, respectively. As-prepared and CO_2-treated samples showed a similar FTIR spectrum. Furthermore, the carbonate peak, which should appear at about 1700 cm^{-1}, was not observed after CO_2 treatment and supports the PXRD chemical stability data. For the H_2O-treated sample, the OH group peak at 3500−3300 cm^{-1} has been observed (Figures 6 and S2 (see Supporting Information)). We also made a similar type of observation for our previously reported Ta-doped BCN,[20] and other acceptor-doped perovskite-type structures, including $BaCe_{0.5}Zr_{0.35}Sc_{0.1}Zn_{0.05}O_{3-\delta}$,[14] La-doped BCY,[26] and $Sr_6Ta_2O_{11}$.[27] The presence of the OH signal in FTIR confirms that the investigated materials absorb protons, and its occupation site in the crystal structure is not known to us presently. It is also important to mention that Zr doping in $BaCe_{1-x}Y_xO_{3-\delta}$ (BCY) also improved the chemical stability in CO_2 and H_2O, which may be attributed to the difference in the bond strength between Zr−O and Ce−O.

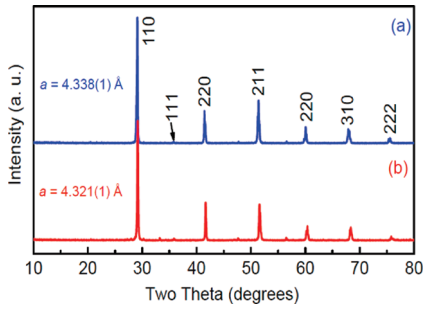

Figure 3. PXRD of (a) $BaCe_{0.8}Zr_{0.1}Nb_{0.1}O_{3\pm\delta}$ and (b) $BaCe_{0.7}Zr_{0.2}Nb_{0.1}O_{3\pm\delta}$ prepared at 1500 °C in air.

Electronic Structure of Ce in Investigated Perovskites. Electron paramagnetic resonance (EPR) spectra of $BaCe_{1-x}Nb_xO_{3\pm\delta}$ and $BaCe_{0.9-x}Zr_xNb_{0.1}O_{3\pm\delta}$ were investigated to probe the nature of the electronic state in the perovskites. Very interestingly, we observed six EPR signals for all the investigated compounds (Figure 7). The EPR signals at $g \simeq 1.964$ and 1.946 (indicated as ε and φ) appear to be characteristic of Ce^{3+} ions since a similar spectra was reported for reduced $CeO_{2-\delta}$.[28,29] We synthesized and investigated the perovskite-type metal oxides at an elevated temperature of 1500 °C in air, which could trigger the reduction process of Ce^{4+} to Ce^{3+} due to the loss of oxygen in the structure. In addition, the signals with factors $g \simeq 2.072$, 2.042, and 2.003 indicated as β, χ, and δ, respectively, are similar to those assigned to oxide-ion species bounded to Ce^{4+} ions.[28,29] The most interesting feature is the presence of the half-field transition signal with $g \simeq 4.203$ (indicated as α), which has also been reported for K- and Pb-doped $Ba_{1-x}K_xBiO_3$ and $BaPb_yBi_{1-y}O_3$[30,31] and ascribed to oxygen ions with different effective charges.

Electrical Conductivity. Figure 8 shows the typical AC impedance plots of $BaCe_{0.8}Zr_{0.1}Nb_{0.1}O_{3\pm\delta}$ and $BaCe_{0.7}Zr_{0.2}Nb_{0.1}O_{3\pm\delta}$ in a variety of atmospheres at 600 °C. Comparable data plots were observed for $BaCe_{0.9}Nb_{0.1}O_{3\pm\delta}$ and $BaCe_{0.8}Nb_{0.2}O_{3\pm\delta}$ over the investigated range of temperature (Figure S3, see Supporting Information). The impedance plots could be described by using an equivalent circuit consisting of the elements (R_b) (R_{gb}, CPE_{gb}) ($R_{el}CPE_{el}$), where R_b, R_{gb}, CPE_{gb}, and CPE_{el} represent bulk resistance, grain-boundary resistance, constant phase element due to grain boundary, and constant phase element due to electrode, respectively (Figure 8a). The grain-boundary and electrode CPE values were found to be on the order of 10^{-8} and 10^{-4}−10^{-3} F at 600 °C, in air, wet H_2, wet N_2, and N_2 saturated with D_2O, respectively. These values fall in the range reported for similar phenomenon in polycrystalline ceramics.[32,33]

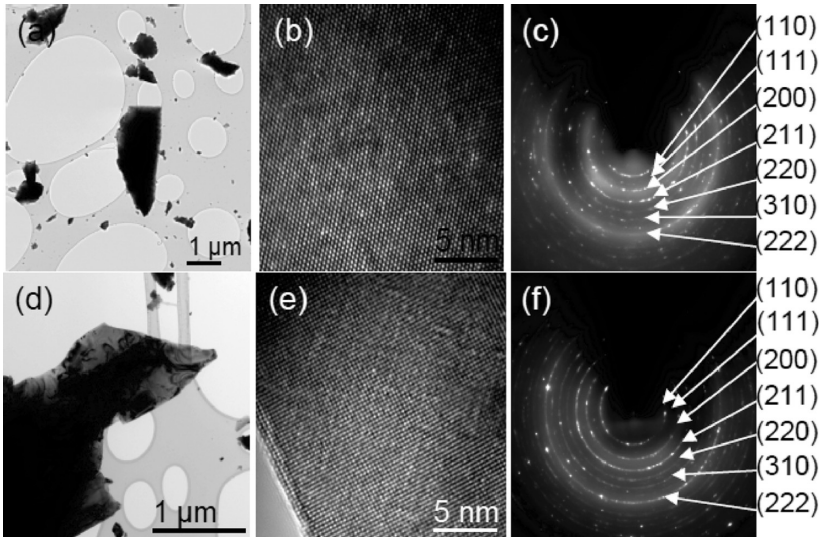

Figure 4. $BaCe_{0.8}Zr_{0.1}Nb_{0.1}O_{3\pm\delta}$ (a−c) and $BaCe_{0.7}Zr_{0.2}Nb_{0.1}O_{3\pm\delta}$ (d−f) show the corresponding TEM and HRTEM images and selected area ED of the sample prepared at 1500 °C in air.

dx.doi.org/10.1021/ic201008v |Inorg. Chem. 2011, 50, 6493–6499

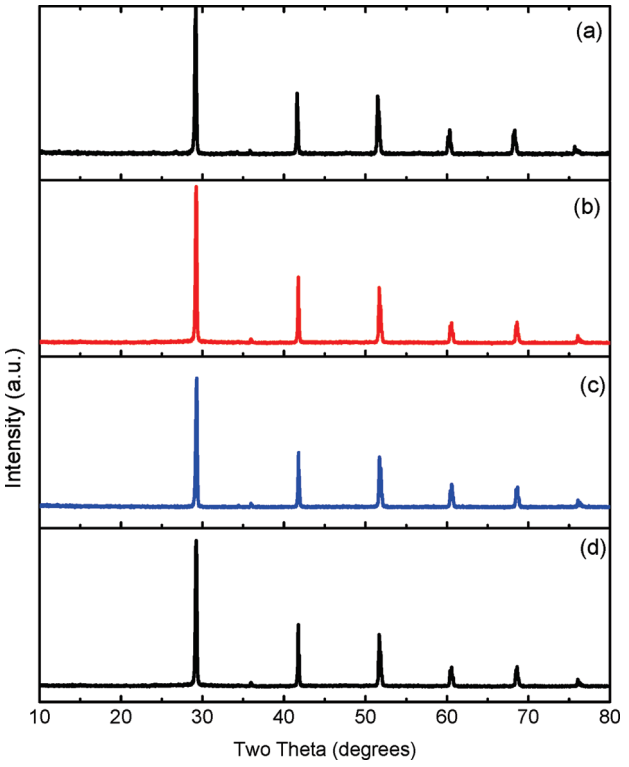

Figure 5. PXRD of $BaCe_{0.8}Zr_{0.1}Nb_{0.1}O_{3\pm\delta}$ after being treated (a) with N_2 + CO_2 (50:50) at 700 °C for 20 h and (b) boiling H_2O for 24 h; (c and d) corresponding data for $BaCe_{0.7}Zr_{0.2}Nb_{0.1}O_{3\pm\delta}$.

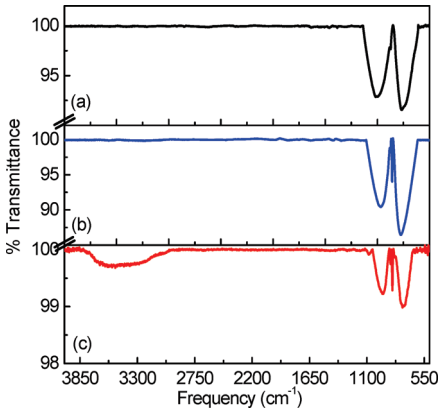

Figure 6. FTIR spectra of $BaCe_{0.8}Zr_{0.1}Nb_{0.1}O_{3\pm\delta}$: (a) as prepared at 1500 °C in air, (b) N_2 + CO_2 (50:50) at 700 °C for 20 h, and (c) boiling H_2O treated sample for 24 h.

We have consistently taken the high-frequency intercept as a bulk (R_b) and the intermediate frequency intercept as being equal to the sum of the total ($R_b + R_{gb}$) to calculate the total conductivity of the investigated perovskites.

Figure 9 shows the plot of $\log_{10}\sigma$ vs $1000/T$ for the total and bulk electrical conductivity of $BaCe_{0.8}Zr_{0.1}Nb_{0.1}O_{3\pm\delta}$ and $BaCe_{0.7}Zr_{0.2}Nb_{0.1}O_{3\pm\delta}$ in air, humidified N_2, and H_2. Figure S4 (see Supporting Information) shows the corresponding data for $BaCe_{0.9}Nb_{0.1}O_{3\pm\delta}$ and $BaCe_{0.8}Nb_{0.2}O_{3\pm\delta}$ in air and wet N_2. In wet N_2 and wet H_2 (3% H_2O), a higher bulk and total conductivity was observed compared to air over the investigated

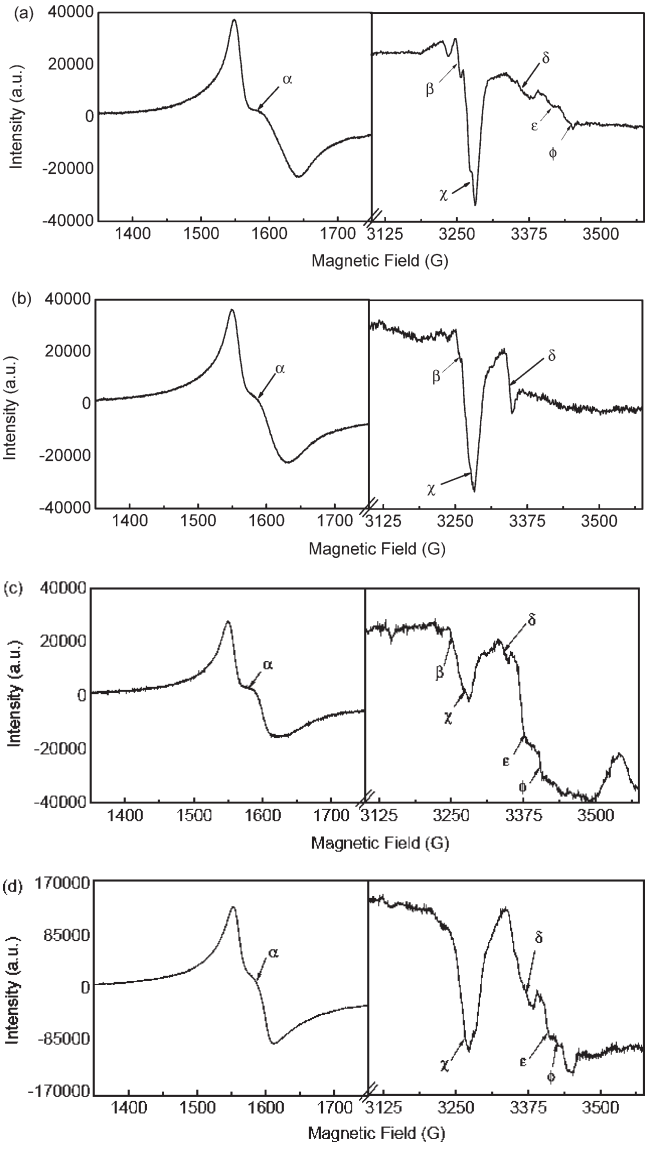

Figure 7. EPR spectra reordered at 108 K for as-prepared (a) $BaCe_{0.9}Nb_{0.1}O_{3\pm\delta}$, (b) $BaCe_{0.8}Nb_{0.2}O_{3\pm\delta}$, (c) $BaCe_{0.8}Zr_{0.1}Nb_{0.1}O_{3\pm\delta}$, and (d) $BaCe_{0.7}Zr_{0.2}Nb_{0.1}O_{3\pm\delta}$. The symbols represent EPR signals with factor g values.

temperature range for Zr+Nb-codoped samples. It is also noted that the bulk and total conductivity in all the investigated atmospheres decreases with increasing Nb in $BaCeO_3$ (Figure S4, see Supporting Information) and also due to Zr doping (Figure 9). For comparison, the electrical conductivity of the parent compound $BaCeO_3$ in air, wet N_2, and wet H_2 was measured (Figure 9), which clearly shows that the Nb+Zr-codoped $BaCe_{0.7}Zr_{0.2}Nb_{0.1}O_{3\pm\delta}$ has a high total electrical conductivity. The electrical conductivity data in air and 3% H_2O + N_2 at 600 °C was found to be the same within experimental error for both $BaCe_{0.9}Nb_{0.1}O_{3\pm\delta}$ and $BaCe_{0.8}Nb_{0.2}O_{3\pm\delta}$ and demonstrates that the humidity do not appear to impact the conductivity in the donor-doped perovskites (Figure S3, see Supporting Information). This can be attributed due to Nb substitution for Ce, which may result in filling of potential oxygen vacancies available for hydration. However, Zr+Nb-codoped samples showed the opposite trend, suggesting that Zr substitution for

dx.doi.org/10.1021/ic201008v |*Inorg. Chem.* 2011, 50, 6493–6499

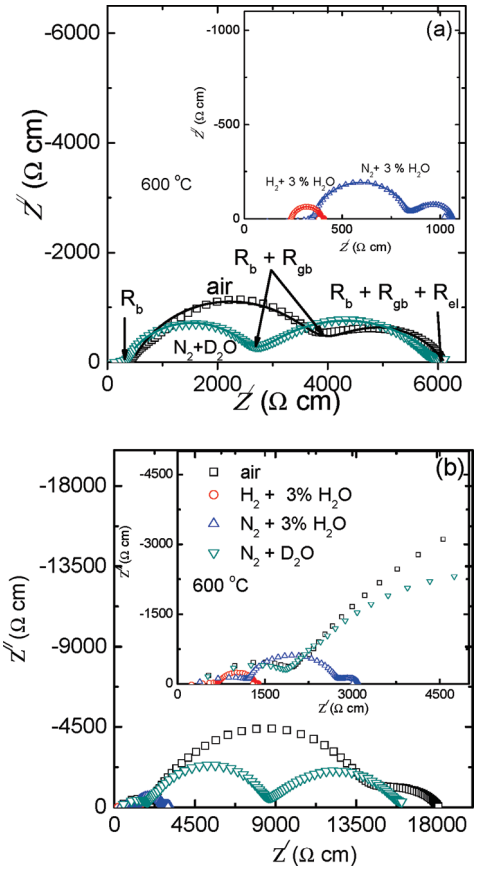

Figure 8. Typical AC impedance plots at 600 °C for (a) $BaCe_{0.8}Zr_{0.1}Nb_{0.1}O_{3\pm\delta}$ and (b) $BaCe_{0.7}Zr_{0.2}Nb_{0.1}O_{3\pm\delta}$ under various atmospheres. The line passing through the data points represents the simulated data using an equivalent circuit consisting of the circuit elements $(R_b)(R_{gb}CPE_{gb})(R_{el}CPE_{el})$ where R_b, R_{gb}, CPE_{gb}, and CPE_{el} represent the bulk resistance, grain-boundary resistance, constant phase element due to grain boundary, and constant phase element due to electrode, respectively.

Ce in $BaCe_{1-x}Nb_xO_{3\pm\delta}$ promotes hydration in the structure (Figure 9) and may suppress the electronic conductivity, especially at low temperatures, due to the presence of Ce^{3+} in the investigated perovskites, which is confirmed by EPR data (Figure 7).

The activation energy for electrical conduction was calculated by fitting the electrical conductivity data to the Arrhenius equation. For our best material $BaCe_{0.8}Zr_{0.1}Nb_{0.1}O_{3\pm\delta}$, we clearly see Arrhenius behavior over the investigated range of 400−700 °C. The activation energy for the bulk conduction was found to be 0.69−0.73 and 1 eV for the total (bulk + grain boundary) conductivity in wet H_2 and wet N_2 and was found to be comparable to that of several proton conducting metal oxides[9,21,38−43] such as $Sr_2Ga_{1.10}Nb_{0.90}O_{6-\delta}$, 0.81 eV,[9] $Ba_{1.75}K_{1.25}CaNb_2O_{9-\delta}$, 1 eV,[21] $Sr_3CaZr_{0.5}Ta_{1.5}O_{8.75}$, 0.85 eV,[38] and Fe-doped $KTaO_3$, 0.88 eV.[39] The compounds with a nominal composition of $BaCe_{1-x}Nb_xO_{3\pm\delta}$ (x = 0.1, 0.2) displayed some non-Arrhenius behavior for the bulk conductivity at high temperature; however, Arrhenius-like behavior was observed for total conductivity (Figure S4, Supporting Information). This result strongly suggests that the bulk conduction mechanism involves a certain degree of a thermal-assisted mechanism. A direct consequence of this motion would be a change in the conduction mechanism at elevated

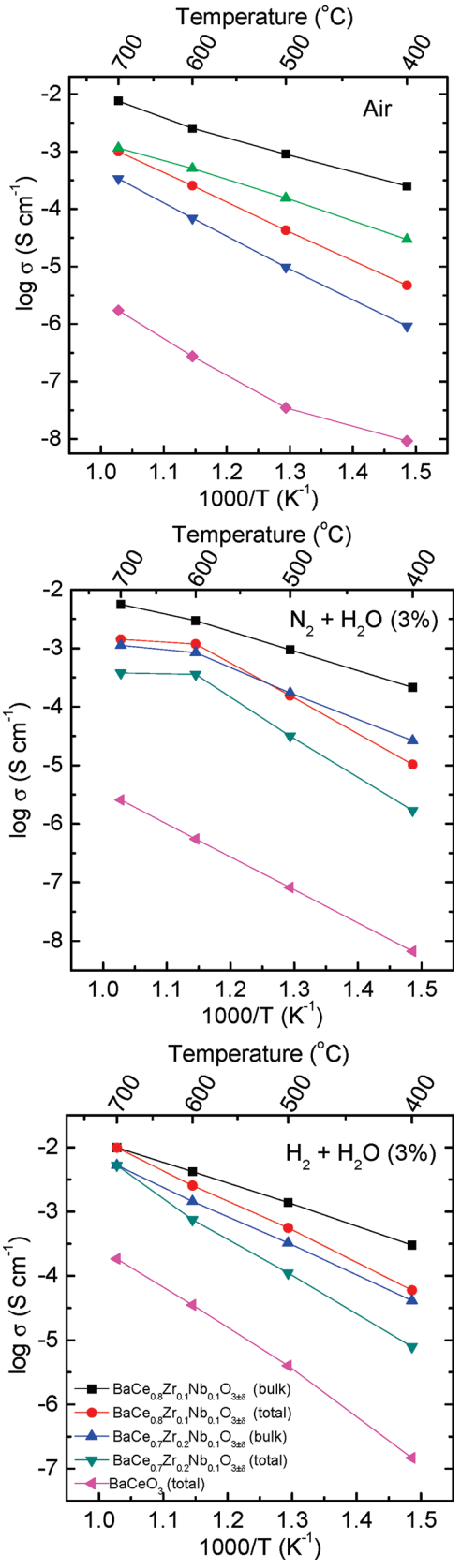

Figure 9. Arrhenius plots for bulk and total (bulk + grain-boundary) electrical conductivity of $BaCe_{0.8}Zr_{0.1}Nb_{0.1}O_{3\pm\delta}$ and $BaCe_{0.7}Zr_{0.2}Nb_{0.1}O_{3\pm\delta}$ in air, wet N_2, and wet H_2. For comparison, total conductivity of the parent compound $BaCeO_3$ is also measured.

dx.doi.org/10.1021/ic201008v |Inorg. Chem. 2011, 50, 6493–6499

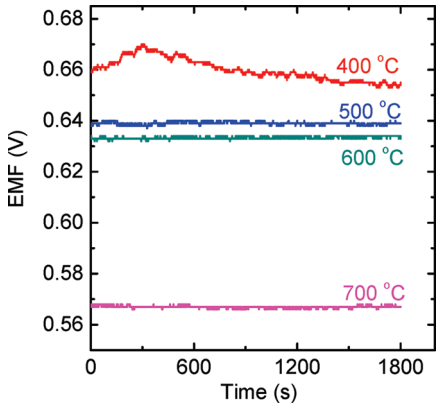

Figure 10. Open-circuit voltage measurements performed over time at different temperatures using the following electrochemical cell: (−) H_2 + 3% H_2O, Pt|$BaCe_{0.8}Zr_{0.1}Nb_{0.1}O_{3\pm\delta}$|Pt, air (+).

temperatures, which may also result in lowering the electrical conductivity due to the disorder at various interstitial sites.

In the literature,[39,44,45] the elementary reactions underlying the mobility of protonic defects have been investigated experimentally[44] as well as by molecular dynamics (MD) simulations,[45] which indicate the possibility of a rotational diffusion transport mechanism for the protonic defect and proton transfer toward a neighboring oxide ion. In this process, the proton shows long-range diffusion whereas the oxygen atoms of the octahedral reside on their lattice positions.[45] The rotational diffusion mechanism for the proton transport is fast with low activation energy barriers, suggesting that the proton transfer reaction appears to be a rate-limiting step in the perovskites.

The origin of proton conduction in high-temperature acceptor-doped perovskites has been investigated by many authors, who established that the conduction occurs by means of interaction of oxide-ion vacancies and water vapor.[5,6,46,47] In the present case, the increase in the electrical resistance under N_2 + D_2O (Figure 8) may confirm that the charge carriers appear to be "protons" in the investigated perovskites. To further confirm the potential ionic (proton) conduction in these donor-doped $BaCeO_3$, the potential of our best chemical composition of $BaCe_{0.8}Zr_{0.1}Nb_{0.1}O_{3\pm\delta}$ was used to build a membrane−electrode assembly (MEA). The electromotive force (EMF) of the H_2 +3% H_2O and air cell was measured as a function of temperature. The MEA was prepared by attaching the Pt wires to porous Pt electrodes on both sides of the pellet. Interestingly, EMF measurements (Figure 10) showed an open-circuit voltage (OCV) of 0.66 V at 400 °C. However, the magnitude of OCV was quite low compared to the theoretical value for water formation, suggesting mixed conduction. It is also important to mention that the Haile group reported proton conduction in oxygen excess perovskites.[48]

CONCLUSIONS

In summary, the present work showed that the perovskite-type $BaCe_{1-x}Nb_xO_{3\pm\delta}$ and $BaCe_{0.9-x}Zr_xNb_{0.1}O_{3\pm\delta}$ can be synthesized using conventional solid-state reactions at elevated temperatures in air. Formation of a single-phase structure was confirmed using powder X-ray diffraction (PXRD) and electron diffraction (ED). The lattice constant was found to decrease with increasing Nb content in $BaCe_{1-x}Nb_xO_{3\pm\delta}$. $BaCe_{0.9}Nb_{0.1}O_{3\pm\delta}$ and $BaCe_{0.8}Nb_{0.2}O_{3\pm\delta}$ were found to be chemically unstable against the reaction with CO_2 at elevated temperatures, while partial Zr substitution for Ce was found to be stable in CO_2. The electrical conductivity of the investigated perovskites showed a mixed ionic and electronic conduction and a significant increase in electrical conduction in H_2-containing atmosphere. Among the compounds investigated, $BaCe_{0.8}Zr_{0.1}Nb_{0.1}O_{3\pm\delta}$ showed the highest bulk electrical conductivity of 1.3×10^{-3} S cm^{-1} and total (bulk + grain-boundary) conductivity of 5.6×10^{-4} S cm^{-1} under wet H_2 at 500 °C, which is comparable to chemically unstable acceptor-doped $BaCeO_3$ and other perovskite-type proton conductors.

ASSOCIATED CONTENT

Supporting Information. This material is available free of charge via the Internet at http://pubs.acs.org.

AUTHOR INFORMATION

Corresponding Author

*Phone: 001 403 210 8649. Fax 001 403 289 9488. E-mail: vthangad@ucalgary.ca (V.T.) and rpaul@ucalgary.ca (R.P.)

ACKNOWLEDGMENT

The authors thank the Natural Sciences and Engineering Research Council of Canada (NSERC) and the Candia Foundation for Innovation for their financial support. The critical comments of one of the Reviewers helped clarify the electrical transport properties of the investigated donor-doped perovskites.

REFERENCES

(1) Iwahara, H.; Esaka, T.; Uchida, H.; Maeda, N. *Solid State Ionics* **1981**, *3*−*4*, 359.
(2) Uchida, H.; Maeda, N.; Iwahara, H. *Solid State Ionics* **1983**, *11*, 117.
(3) Norby, T. *Solid State Ionics* **1999**, *125*, 1.
(4) Kreuer, K. D. *Chem. Mater.* **1996**, *8*, 610.
(5) Iwahara, H. *Solid State Ionics* **1995**, *77*, 289.
(6) Iwahara, H. *Solid State Ionics* **1996**, *86*−*88*, 9.
(7) Bonanos, N. *Solid State Ionics* **2001**, *145*, 265.
(8) Paddison, S. J.; Paul, R.; Zawodzinski, T. A. *J. Chem. Phys.* **2001**, *115*, 7753.
(9) (a) Liang, K. C.; Nowick, A. S. *Solid State Ionics* **1993**, *61*, 77. (b) Kui, X.; Ruiqiang, Y.; Xiaoxiang, X.; Xingqin, L.; Guangyao, M. *Mater. Res. Bull.* **2009**, *44*, 1474. (c) Kui, X.; Ruiqiang, Y.; Xiaorui, C.; Dehua, D.; Songlin, W.; Xingqin, L.; Guangyao, M. *J. Alloys Compd.* **2009**, *472*, 551.
(10) Liang, K. C.; Du, Y.; Nowick, A. S. *Solid State Ionics* **1994**, *69*, 117.
(11) Nowick, A. S.; Du, Y. *Solid State Ionics* **1995**, *77*, 137.
(12) Nowick, A. S.; Du, Y.; Liang, K. C. *Solid State Ionics* **1999**, *125*, 303.
(13) Krug, F.; Schober, T. *Solid State Ionics* **1996**, *92*, 297.
(14) Schober, T.; Krug, F.; Schilling, W. *Solid State Ionics* **1997**, *97*, 369.
(15) Valkenberg, S.; Bohn, H. G.; Schilling, W. *Solid State Ionics* **1997**, *97*, 511.
(16) Schober, T.; Friedrich, J. *Solid State Ionics* **2000**, *136*−*137*, 161.
(17) Wang, W.; Virkar, A. V. *J. Electrochem. Soc.* **2003**, *150*, A92.
(18) Wang, W.; Virkar, A. V. *J. Electrochem. Soc.* **2004**, *150*, A1565.
(19) Irvine, J. T. S.; Corcoran, D. J. D.; Vazquez, J. C. *Solid State Ionics* **2002**, *152*−*153*, 749.
(20) Bhella, S. S.; Thangadurai, V. *J. Power Sources* **2009**, *186*, 311.
(21) Bhella, S. S.; Thangadurai, V. *Solid State Ionics* **2011**, *192*, 229.

(22) (a) Dauter, J.; Maffei, N.; Bhella, S. S.; Thangadurai, V. *J. Electrochem. Soc.* **2010**, *157*, B1413. (b) Trobec, F.; Thangadurai, V. *Inorg. Chem.* **2008**, *47*, 8972.
(23) Katahira, K.; Kohchi, Y.; Shimura, T.; Iwahara, H. *Solid State Ionics* **2000**, *138*, 91.
(24) Fabbri, E.; Pergolesi, D.; Epifanio, A. D.; Bartolomeo, E. D.; Balestrino, G.; Licoccia, S.; Traversa, E. *Energy Environ. Sci.* **2008**, *1*, 355.
(25) Brixner, L. *J. Inorg. Nucl. Chem.* **1960**, *15*, 352.
(26) Kruth, A.; Davies, R. A.; Islam, M. S.; Irvine, J. T. S. *Chem. Mater.* **2007**, *19*, 1239.
(27) Raj, E. S.; Skinner, S. J.; Kilner, J. A. *Solid State Ionics* **2005**, *176*, 1097.
(28) Oliva, C.; Termignone, G.; Vatti, F. P.; Forni, L.; Vishniakov, A. V. *J. Mater. Sci.* **1996**, *31*, 6333.
(29) Abi-aad, E.; Bechara, R.; Grimblot, J.; Aboukais, A. *Chem. Mater.* **1993**, *5*, 793.
(30) Yakuboskii, A. Yu.; Gudenko, S. V.; Anshukova, N. V.; Golovashkin, A. I.; Ivanova, L. I.; Rusakov, A. P. *J. Exp, Theor, Phys,* **1999**, *88*, 732.
(31) Golovashkin, A. I.; Yakubovskii, A.; Gudenko, S.; Rusakov, A. P. *Physica C* **1999**, *317*−*318*, 432.
(32) Atamanik, E.; Thangadurai, V. *Mater. Res. Bull.* **2009**, *44*, 931.
(33) Irvine, J. T. S.; Sinclair, D. C.; West, A. R. *Adv. Mater.* **1990**, *2*, 132.
(34) Azad, A. K.; Irvine, J. T. S. *Solid State Ionics* **2007**, *178*, 635.
(35) Tao, S.; Irvine, J. T. S. *J. Solid State Chem.* **2007**, *180*, 3493.
(36) Iguchi, F.; Sata, N.; Tsurui, T.; Yugami, H. *Solid State Ionics* **2007**, *178*, 691.
(37) Baik, H. D. *J. Korean Ceram. Soc.* **2002**, *39*, 635.
(38) Potter, A. R.; Baker, R. T. *Solid State Ionics* **2006**, *177*, 1917.
(39) Kreuer, K. D. *Annu. Rev. Mater. Res.* **2003**, *33*, 333.
(40) Corcoran, D. J. D.; Irvine, J. T. S. *Solid State Ionics* **2001**, *145*, 307.
(41) Scherban, T.; Nowick, A. S. *Solid State Ionics* **1992**, *53*−*56*, 1004.
(42) Klauer, S.; Whohlecke, M.; Kapphan, S. *Phys. Rev. B* **1992**, *45*, 2786.
(43) Balakireva, V. B.; Gorelov, V. P. *Solid State Ionics* **1998**, *36*, 217.
(44) Pionke, M.; Mono, T.; Schweika, W.; Springer, T.; Schober, T. *Solid State Ionics* **1997**, *97*, 497.
(45) Kreuer, K. D.; Munch, W.; Traub, U.; Maier, J. *Ber. Bunsen Ges. Phys. Chem.* **1998**, *102*, 552.
(46) Glöckner, R.; Islam, M. S.; Norby, T. *Solid State Ionics* **1999**, *122*, 145.
(47) Kruth, A. R.; Davies, A.; Islam, M. S.; Irvine, J. T. S. *Chem. Mater.* **2007**, *19*, 1239.
(48) Shima, D.; Haile, S. M. *Solid State Ionics* **1997**, *97*, 443.